Title

Astrocyte endfoot formation controls the termination of oligodendrocyte precursor cell perivascular migration during development.

Journal

Neuron, 111(2)

Authors

Su, Yixun
Wang, Xiaorui
Yang, Yujian
et al.

Publication Date

2023-01-18

DOI

10.1016/j.neuron.2022.10.032

Peer reviewed

HHS Public Access

Author manuscript

Neuron. Author manuscript; available in PMC 2024 January 18.

Published in final edited form as:

Neuron. 2023 January 18; 111(2): 190–201.e8. doi:10.1016/j.neuron.2022.10.032.

Astrocyte endfoot formation controls the termination of oligodendrocyte precursor cell perivascular migration during development

Yixun Su[1,2], **Xiaorui Wang**[1], **Yujian Yang**[1,3], **Liang Chen**[4], **Wenlong Xia**[5], **Kimberly K. Hoi**[5], **Hui Li**[1,2], **Qi Wang**[1,2], **Guangdan Yu**[1], **Xiaoying Chen**[1], **Shouyu Wang**[1], **Yuxin Wang**[1], **Lan Xiao**[1], **Alexei Verkhratsky**[6,7], **Stephen P.J. Fancy**[*,5], **Chenju Yi**[*,2], **Jianqin Niu**[*,1,8]

[1]Department of Histology and Embryology, Chongqing Key Laboratory of Neurobiology, Brain and Intelligence Research Key Laboratory of Chongqing Education Commission, Third Military Medical University, Chongqing 400038, China

[2]Research Centre, Seventh Affiliated Hospital of Sun Yat-sen University, Shenzhen 518107, China

[3]Department of Ophthalmology, Army Specialty Medical Center, Third Military Medical University, Chongqing 400042, China

[4]Department of Orthopedics, Army Specialty Medical Center, Third Military Medical University, Chongqing 400042, China

[5]Department of Neurology, Department of Pediatrics, Division of Neuroimmunology and Glial Biology, Newborn Brain Research Institute, University of California at San Francisco, San Francisco, CA 94158, USA

[6]Faculty of Biology, Medicine and Health, The University of Manchester, Manchester M139PL, UK

[7]Achucarro Center for Neuroscience, IKERBASQUE, Bilbao 48011, Spain

[8]Lead contact

Summary:

Oligodendrocyte precursor cells (OPCs) undergo an extensive and coordinated migration in the developing CNS, using the pre-formed scaffold of developed blood vessels as their physical substrate for migration. Whilst OPC association with vasculature is critical for dispersal, equally

[*]Correspondence: stephen.fancy@ucsf.edu (S.P.J.F.), yichj@mail.sysu.edu.cn (C.Y.), jianqinniu@tmmu.edu.cn (J. N.).

Author contributions

J.N., C.Y. and S.P.J.F. conceived the study. J.N., C.Y. and S.P.J.F. designed the experiments. Y.S., X.W., Y.Y., W.X., K.K.H., H.L., Q.W., G.Y., X.C., S.W., Y.W. and J.N. performed the experiments and analyzed the data. L.C. assisted with live imaging experiments. Y.S. and Q.W. performed analysis of the Mass spectrometry data. L.X. contributed to discussion. A.V. helped design some of the experiments and contributed to discussion. J.N., C.Y. and S.P.J.F. wrote the manuscript. S.P.J.F. made the editing.

Competing interests

The authors declare no competing interests.

important for permitting differentiation and proper myelination of target axons is their appropriate and timely detachment, but regulation of this process remains unclear. Here we demonstrate a correlation between the developmental formation of astrocytic endfeet on vessels and the termination of OPC perivascular migration. Ex vivo and in vivo live imaging show astrocyte endfeet physically displace OPCs from vasculature, and genetic abrogation of endfoot formation hinders both OPC detachment from vessels and subsequent differentiation. Astrocyte-derived semaphorins 3a and 6a act to repel OPCs from blood vessels at the cessation of their perivascular migration, and in so doing, permit subsequent OPC differentiation by insulating them from a maturation inhibitory endothelial niche.

In Brief

Su et al. find that the developmental placement of astrocyte endfeet on vessels controls the termination of widespread OPC perivascular migration. Astrocytes produce semaphorins 3a and 6a which repel OPCs from the vasculature, and permit their subsequent differentiation by releasing them from a maturation inhibitory endothelial niche.

Graphical Abstract

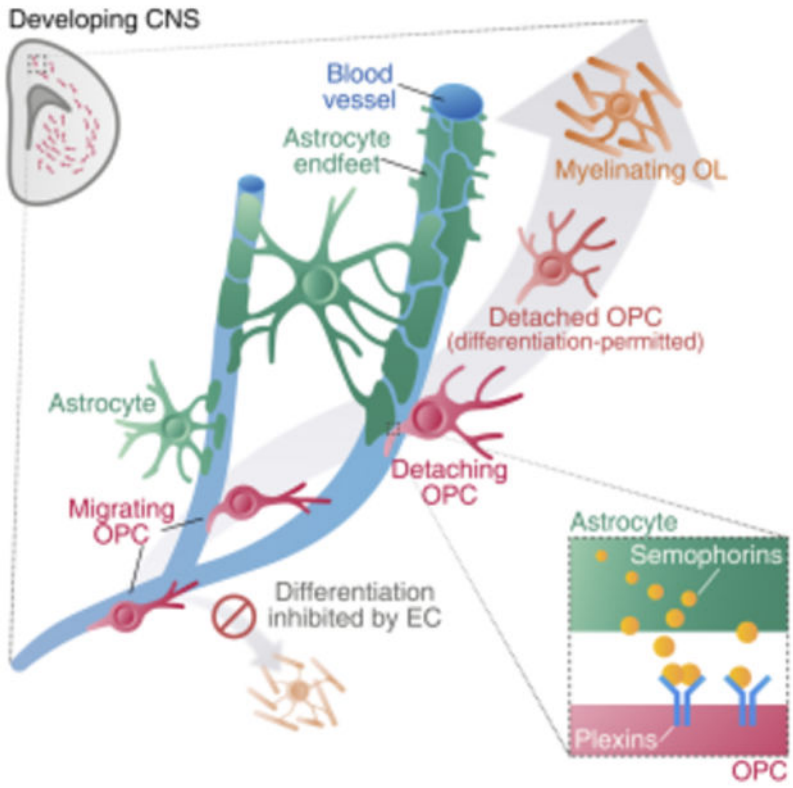

Keywords

oligodendrocyte precursor cells; perivascular migration; astrocyte endfoot; semaphorins; myelination

Introduction:

The adult mammalian CNS requires establishment of intricate functional interactions between neurons and glia. Oligodendrocytes (OL), the myelinating cells of the CNS, have critical roles in maintaining axon integrity and allowing for rapid saltatory nerve conduction (Funfschilling et al., 2012; Lee et al., 2012). The uniform distribution of OL throughout the adult CNS is therefore critical, but their founder oligodendrocyte precursor cells (OPCs) arise developmentally from restricted ventricular zone domains in brain and spinal cord (Kessaris et al., 2006; Lu et al., 2002; Tekki-Kessaris et al., 2001). In the spinal cord, OPC development is initiated in the same motor neuron progenitor domain (pMN) that gives rise to motor neurons. pMN precursors give rise in a first wave to motor neuron progeny (from about embryonic day (E) 9–10.5 in the mouse), and subsequently in a later wave of OPCs (E12.5) (Glial cell development : basic principles and clinical relevance, 2001; Miller, 2002). Later in development a second smaller source of OPCs arises from a discrete location in the dorsal spinal cord (Cai et al., 2005). In the mouse brain, OPCs seem to arise in three waves, firstly from the medial ganglionic eminence (MGE) and anterior entopeduncular area (AEP) in the ventral forebrain, secondly from the lateral and/or caudal ganglionic eminences (LGE and CGE), and a third later wave originating within the postnatal cortex (Kessaris *et al.*, 2006). From these developmental origins, OPCs undergo an extensive and coordinated migration before halting appropriately to tile the CNS (Hughes et al., 2013; Tsai et al., 2002) or differentiate and myelinate their target axons. A variety of factors have been implicated in regulating the developmental migration of OPCs, both in providing guidance (Jarjour and Kennedy, 2004; Xia and Fancy, 2021) and regulating their motility (Xia and Fancy, 2021), as well as in regulating the timing of migration cessation (Tsai *et al.*, 2002). It was unclear however whether there were highly defined pre-existing substrates that provide guidance for OPC migration. Recent evidence has shown that widespread OPC dispersal in development is mediated using vasculature as a physical substrate for migration. OPCs utilize and require vessels for their distribution throughout the CNS, which involves direct contact with the abluminal endothelial surface. Whilst OPC association with vasculature is critical for their dispersal, and mediators of attraction to the endothelium have been identified (Tsai et al., 2016), equally important for permitting OPC differentiation and proper CNS myelination is the regulation of their appropriate and timely vascular detachment. Little is understood about regulation of the termination of OPC perivascular detachment. Here we show that astrocyte endfoot placement in development and astrocyte derived Sema3a and 6a mediated repulsion of OPCs is a critical mechanism in controlling termination of OPC perivascular migration, and permitting subsequent differentiation by displacing OPCs from an inhibitory endothelial niche.

Results:

Astrocyte endfoot formation correlates with the termination of OPC perivascular migration.

To investigate potential mechanisms contributing to the termination of OPC perivascular migration, we examined positional relationships between various cell types and the vasculature in developing mouse brain tissues. In the embryonic brain, OPCs migrate in two waves (from MGE/AEP, then LGE/CGE), from ventral to dorsal along the vascular

scaffold. We found a strong spatiotemporal correlation between the formation of astrocyte endfeet and the dissociation of OPCs from microvessels at the conclusion of this migration. Using lectin to stain microvessels in the embryonic double reporter mouse strain Aldh1l1-eGFP:NG2-creER:R26-LSL-tdTomato (in which astrocytes and their endfeet are eGFP+, whereas OPCs are tdTomato+), we found that astrocyte endfoot formation on vessels also follows a spatiotemporal sequence of 'ventral brain-lateral-dorsal' (Figures 1A and 1B) as reported previously (Fallier-Becker et al., 2014). During this endfoot investment, we found that juxtavascular (with cell body contacting vessel) tdTomato+ OPCs contacted only lectin-labeled blood vessels devoid of eGFP+ astrocyte endfeet. Astrocyte endfeet seemed to interpose between OPCs and vessels (Figure 1C; Figure S1A), and quantification at embryonic times showed a distinct negative correlation between astrocyte endfoot formation and the percentage of juxtavascular OPCs (coefficient of determination Pearson's r=−0.960, Figures 1D and 1E). During early postnatal development a third later wave of OPCs originating within the postnatal cortex undergoes perivascular migration from deep to superficial layers. We found a similar negative correlation in postnatal dorsal cortex between percentage of juxtavascular OPCs and astrocyte endfoot formation (P4 to P10, Pearson's r=−0.822, Figures 1F and 1G). This correlation was also found in different brain regions, including lateral cortex and caudate putamen (Pearson's r=−0.786 and −0.719, respectively) (Figure 1G). There appears to be no correlation between the timing of pericyte investment on vessels (which precedes OPC migration) and the cessation of OPC perivascular migration (Figure S1B). Additionally, microglia and axonal signaling do not seem to participate in cessation of this migration (Figures S1C and S1D). Together, our results show that OPC dissociation from vasculature at the conclusion of their perivascular migration correlates spatiotemporally with astrocyte endfoot formation in CNS development (Figure 1M).

Astrocyte endfoot formation mediates OPC perivascular detachment.

OPC vascular detachment occurs frequently in the mouse cortex at P5, as third wave migrating OPCs complete their perivascular migration, and is a time when Aldh1l1-GFP+ astrocytes (in Aldh1l1-eGFP:NG2-creER:R26-LSL-tdTomato mice) begin to have processes interposing between the vessel and tdTomato+ (or PDGFRα+) OPCs. To assess the interaction between astrocytes and perivascular OPCs at the vascular surface, we made use of both ex vivo and in vivo live imaging of Aldh1l1-eGFP:NG2-creER:R26-LSL-tdTomato mice. These mice were treated with tamoxifen at P2–3 and intravenously injected with Lectin-AF649 to label vessels, immediately before imaging at P5. For ex vivo live imaging, cortical slices were prepared and imaged over a period of 360 minutes. Live imaging showed examples of astrocyte endfeet forming and contacting vessels, and these astrocyte processes interposing between vessel and juxtavascular OPC (Figures 1H and 1I; Movie S1); Quantification of this live imaging in acute brain slices showed that 92.3 ± 3.9% of OPC detachments (A total of 19 out of 21 cells in 4 experiments) appeared to involve participation of astrocyte endfeet (Figure 1J). Similar phenomena of astrocyte endfoot formation displacing juxtavascular OPCs from the vessel could also be observed by *in vivo* live imaging (Figures 1K and 1L; Movie S2).

To assess a functional requirement for astrocyte endfoot formation in regulating OPC vascular detachment, we made use of a modified astrocyte laser-ablation model (Kubotera

et al., 2019), as published previously. In this model, Aldh1l1-eGFP labeled astrocytes (labelling 97.95±0.46% of all BLBP+ astrocytes) near the surface of the dorsal cortex were ablated using a two-photon laser in P5 mice, and tissue was collected 24 hours later (Figures 2A and 2B). This laser ablation protocol led to focal loss of astrocytes in the dorsal cortex (Figure 2C). Notably this laser ablation did not alter the number of OPCs (Figures 2D and 2E). It also did not appear to affect the integrity of the vascular unit or blood brain barrier, as evidenced by lack of fibrinogen leakage from its intravascular location (Figures S1E and S1F). Iba1+ microglia also did not appear reactive, as their cell number and morphology were unchanged (Figure S1F). This focal loss of astrocytes in the early postnatal cortex was associated with a marked decrease in the apparent ability of OPCs to detach from vasculature. There was a significant increase in PDGFRα+ and Olig2+ juxtavascular OPCs (as a percentage of total OPCs) in the ablation area with their cell bodies contacting blood vessels (Figures 2F and 2G).

In an alternative approach, we made use of a cell-specific diphtheria toxin A (DTA) expression-based mouse strain (hGFAP-cre:DTA). Surprisingly, the hGFAP-cre:DTA strain did not show significant differences in the number of astrocytes until P11 (Figure 2H), but was associated with a marked defect in astrocyte endfoot formation when compared to littermate controls (non-cre:DTA) as early as P7 (Figures 2H and 2I). This phenotype was also associated with a significant decrease in OPC detachment from vessels at both P7 and P11(Figure 2J), without affecting the total number of OPCs (Figure 2K). Together, these live imaging and functional studies demonstrate a physical interaction between astrocyte endfeet and perivascular OPCs at the vascular surface at the conclusion of perivascular migration, and suggest that astrocyte endfoot formation is a key contributor to OPC detachment from the vasculature.

OPC detachment from vasculature permits their subsequent differentiation.

OPC dispersal in development would seem to need a mechanism to prevent premature differentiation of OPCs while migrating on the vasculature. Indeed, very few committed precursors (ITPR2+) and mature OLs (CC1+) are closely associated with vessels in postnatal cortex compared to NG2 expressing juxtavascular OPCs (Figures 3A and 3B). Endothelial cells and their products also seem to directly inhibit OPC differentiation, as OPCs in vitro treated with endothelial cell conditioned medium, co-cultured with endothelial cells, or seeded on a paraformaldehyde (PFA)-fixed endothelium monolayer, all seemed to have significantly reduced OPC differentiation compared to controls (Figure 3C). In contrast, OPCs co-cultured with 293T cells did not show any reduction in differentiation (Figure S1H).

We also find that altered OPC vascular detachment in vivo affects their differentiation and subsequent myelination. As described above, OPCs show a decreased ability to detach from vessels in the postnatal cortex of hGFAP-cre:DTA mice (in which astrocyte numbers appear unaltered but there is markedly reduced astrocyte endfoot formation). This phenotype is accompanied by significant suppression of OPC differentiation, as indicated by the inhibited expression of mature oligodendrocyte markers PLP and MBP (Figures 3D and 3E), without impacting IBA1+ microglia numbers or CD31+ vascular morphology (Figure S1G). These

results indicate that the endothelium inhibits OPC differentiation during their perivascular migration, and that detachment from vasculature is needed to permit their subsequent maturation.

Astrocyte semaphorins 3a and 6a repel OPCs from vasculature *in vivo*

To interrogate potential mechanisms of astrocyte mediated OPC vascular detachment, we procured a proteomic profile of acutely isolated astrocytes, OPCs and OLs at P7 using mass spectrometry, and analyzed the interactions between astrocyte-enriched extracellular/membrane proteins and OPC-enriched membrane proteins using the STRING database (Szklarczyk et al., 2021) (Figures S2A and S2B). Gene ontology_Molecular Function (GO_MF) enrichment analysis showed that the interaction network was primarily enriched in protein binding, semaphorin receptor activity and others (Figures S2B and S2C). Among these candidates, the interaction between astroglial semaphorins (Sema6a, Sema7a) and OPC expressed plexins (Plxna2, Plxnd1) was notable, as semaphorin receptor activity has both high enrichment confidence ($p = 2.98 \times 10-8$, 2nd highest) and high fold-enrichment (67.1-fold, 3rd highest) when compared to other GO_MF terms (Figure S2C). Semaphorin-plexin interactions have been reported to mediate chemoattraction/repulsion in a wide range of tissues, and semaphorins (Sema3a, 6d, and 4d) have been found to repel OPCs in white matter injury (Bernard et al., 2012; Boyd et al., 2013; Leslie et al., 2011; Syed et al., 2011; Williams et al., 2007; Yamaguchi et al., 2012). We speculated that astrocytic semaphorins might be responsible for repelling OPCs from vessels during the termination of their perivascular migration.

We performed RT-qPCR to analyze the expression of semaphorins in different brain cell types during development. Among them, Sema3a, 6a, and 7a showed higher expression levels in astrocytes than in other cell types at both early (P5) and late (P28) developmental stages (Figure S2D). Their astrocytic expression was further confirmed by super-resolution fluorescence microscopy in P5 mouse brain (Figures S2F and S2H). A wide range of semaphorin receptors, such as Plxna1/a2/a4 (Sema3a/6a receptors), Plxnc1 (Sema7a receptor), Plxnd1 (Class3/4 semaphorin receptor) and Nrp1 (Semaphorin co-receptor) (Kruger et al., 2005; Takamatsu and Kumanogoh, 2012), were all found to be expressed by OPCs (Figures S2E, S2G and S2I), suggesting that OPCs may respond to different semaphorins in a context dependent manner. Based on our analysis and previous studies, we interrogated astroglial Sema3a, 6a or 7a for their role in repelling OPCs from vasculature.

To assess effects of astrocytic Sema3a, 6a, and 7a on OPCs, we performed in vitro OPC transwell migration assays and agarose dot assays. We found that all three of these semaphorins act to repel OPCs in vitro. OPCs were impeded to migrate into semaphorin-containing lower chambers in the transwell migration assay (Figure S3A), and were repelled away by semaphorin-containing drops in the agarose dot assay (Figure S3B). Notably, we found that Sema3a, 6a or 7a, when added into the medium up to 200 ng/mL, did not themselves affect OPC differentiation or proliferation *in vitro* (Figures S3C and S3D), in contrast with prior reports (Syed *et al.*, 2011) in which OPC differentiation was inhibited by 5 μg/mL Sema3a in the medium; this concentration being much higher than that in the growth cone collapse assay or migration assay (Luo et al., 1993; Piaton et al., 2011).

Astrocytes have been shown to regulate OPC development in various ways (Nutma et al., 2020). Our approaches using laser ablation and hGFAP-cre:DTA remove astrocytes or have the potential to produce dysfunctional astrocytes. We therefore sought to produce astrocyte specific knockdown of semaphorins in vivo in the presence of otherwise functional astrocytes. This in vivo astrocyte specific knockdown of different semaphorins was achieved by injecting CBG-DIO-miR30shRNA AAV into the cortex of Aldh1l1-CreERT mice at P2 (Figure 4A; Figures S3E–H). Knockdown of Sema3a and Sema6a but not Sema7a in astrocytes resulted in increased OPC-vessel association (Figures 4B and 4C). The lack of effect of Sema7a knockdown suggests that this viral approach itself does not disrupt normal astrocyte function. The ability of Sema3a- and Sema6a-knockdown astrocytes to displace OPCs from the vessels was decreased, when compared to the scrambled shRNA control (Figure 4B, lower panels), without altering astrocyte endfoot formation, vessel length or OPC numbers (Figure 4C). In addition, the combination of Sema3a and 6a knockdown resulted in a similar increase of juxtavascular OPCs as in Sema3a knockdown, suggesting a predominant role for Sema3a in regulation of OPC detachment *in vivo* (Figure 4C). Reduced OPC vascular detachment in astrocytic Sema3a/6a knockdown was sufficient to perturb OPC differentiation. We found that the percentage of ITPR2+ committed precursors was decreased by knockdown of astrocyte Sema3a and Sema6a but not Sema7a at P7 (Figure 4D, E). Similarly, MBP staining at P10 also revealed a hypomyelination under either separate or combined astrocytic Sema3a/6a knockdown (Figure 4D, E).

In a converse approach, we sought to assess astrocyte specific overexpression of Sema3a in vivo by injecting a CMV-DIO-Sema3a-P2A-EGFP-tWPA AAV into the developing cortex of Aldh1l1-CreERT mice at P2 (Figure 4F; Figure S3I and S3J). Astrocyte Sema3a overexpression resulted in increased OPC detachment from vessels without affecting astrocyte endfoot formation, vessel length or OPC numbers (Figure 4G and 4H). This astrocytic Sema3a overexpression also resulted in precocious appearance of ITPR2 and MBP expressing cells as early as P5 (Figure 4I and 4J), suggesting that premature OPC dissociation from vasculature allows for precocious differentiation. Taken together, these findings suggest that astrocytic semaphorins 3a and 6a act to repel OPCs and regulate their vascular detachment.

Discussion:

OPCs migrate more widely than neurons and other glial cells in the developing CNS. They achieve this widespread dispersal, from their restricted ventricular zone origins, using vasculature as the physical substrate for their migration (Tsai *et al.*, 2016). Mechanisms which attract OPCs to the endothelium during this perivascular migration have been reported previously (Tsai *et al.*, 2016). Intrinsic Wnt tone in OPCs is critical for attracting OPCs to the endothelium, and achieves this through upregulation of C-X-C motif chemokine receptor type 4 (Cxcr4) in OPCs, which binds to its ligand Stromal cell-derived factor-1 (Sdf1) on endothelium. Here we report a mechanism of repulsion from the vasculature, as astrocyte endfoot formation and production of Sema3a and 6a acts to displace OPCs away from the endothelium. Evidence for the involvement of the end foot comes from the correlation of the timing of end foot placement with OPC detachment (Figure 1E and 1G), the demonstration of end feet interdigitating between OPC and endothelium (Figure

1C and 1F, Figure S1A and Movie S1, 2), and the likelihood that endfoot placement over endothelium also reduces the availability of endothelial Sdf1 for interaction with Cxcr4 on OPCs (Tsai *et al.*, 2016). In the absence of a genetic or pharmacologic way to solely affect the astrocyte endfeet, it remains difficult to specifically functionally implicate them. It is likely that a fine balance exists between mechanisms of OPC attraction to and repulsion from the endothelium, determining their relative association with vessels. If attractive mechanisms are dysregulated, such as a situation of excessive Wnt tone in OPCs, this can overcome mechanisms of repulsion, leading to accumulation of OPCs on the endothelium, displacement of astrocytes from the vessel, and even subsequent effects on the blood brain barrier (Niu et al., 2019).

Astrocytes have been shown to regulate OPC development in various ways (Nutma *et al.*, 2020). For instance, astrocytic secretory factors (Moore et al., 2011), matrix molecules (Cho et al., 2019) and extracellular vesicles (Willis et al., 2020) have all been shown to facilitate or impede OPC migration, proliferation, differentiation and even survival (de Waard and Bugiani, 2020; Jiang et al., 2016; Meyer-Franke et al., 1999; Tognatta et al., 2020). Here we show a novel role for astrocytes in regulating OPC migration and subsequent differentiation. OPC association with the endothelium prevents their differentiation during migration. The placement of astrocyte endfeet on vessels and Sema 3a/6a repulsive mechanism not only acts to terminate perivascular migration and displace OPCs away from vessels, but also permits subsequent OPC maturation by distancing and shielding them from this maturation inhibitory endothelial niche.

A pool of OPCs remains in adulthood comprising 5% of the cells in the CNS. A key question in oligodendroglial biology surrounds what mechanisms underlie the OPC decision to mature or remain a progenitor during development. Whilst astrocyte endfeet displace juxtavascular OPCs from the endothelium at the termination of perivascular migration, permitting their differentiation, it is interesting to note that adult OPCs retain physical contact with endothelial cells of the vasculature through multiple processes (Figure S4, Movie S3). It will be important to understand more about the nature of these process contacts with the endothelium, and whether continued signaling from the endothelium to OPCs contributes to maintenance of an adult pool of oligodendroglial precursors.

Several guidance signals have been reported to regulate the positioning of OPCs; including semaphorins, netrins, bone morphogenetic proteins (BMPs), C-X-C motif chemokine ligand 1 (CXCL1), Tenascin-C and other growth factors (recently reviewed in (Xia and Fancy, 2021)). Semaphorins are an extracellular signaling family of guidance ligands, including secreted proteins (class 3), transmembrane proteins (class 4–6) and membrane-attached proteins (class 7) (Kruger *et al.*, 2005). Semaphorins participate in many key processes within the developing CNS (Mann et al., 2007), through engagement of their receptors and co-receptors. During oligodendroglial lineage development, Sema3a and 3f have been reported to be involved in cell migration; Sema3a, 4d, 6a and 6d in OPC differentiation; and Sema4a in apoptosis of OL (Bernard *et al.*, 2012; Chiou et al., 2019; Leslie *et al.*, 2011; Spassky et al., 2002; Syed *et al.*, 2011; Yamaguchi *et al.*, 2012). In demyelinating diseases, such as multiple sclerosis, Sema3a, 3f, 6a, 4d and 7a have been suggested to be upregulated in or around demyelinating lesions (Bernard *et al.*, 2012; Giraudon et al., 2004;

Gutiérrez-Franco et al., 2016; Williams *et al.*, 2007), and may integrate with other signals to regulate the recruitment or differentiation of OPCs in remyelination of injured areas. In addition, multiple semaphorin receptors have been identified in OPCs (Kruger *et al.*, 2005), and with development-related expression patterns (Spassky *et al.*, 2002; Sugimoto et al., 2001). Their functions in OPCs seem to depend on the interacting semaphorin ligands, for instance Plxna4 mediates the repelling effect of Sema3a and 6a on OPCs in vivo (Binamé et al., 2019; Okada et al., 2007; Xiang et al., 2012). It remains to be fully understood why both OPCs and astrocytes express multiple semaphorins and receptors, and whether it is a mechanism for OPCs and astrocytes to repel other cells during CNS development.

Star Methods

Resource availability

Lead contact—Further information and requests for resources and reagents should be directed to and will be fulfilled by the lead contact, Jianqin Niu (jianqinniu@tmmu.edu.cn)

Materials availability—All unique/stable reagents generated in this study are available from the Lead Contact without restriction.

Data and code availability

- The mass spectrometry proteomics data have been deposited to the ProteomeXchange Consortium (http://proteomecentral.proteomexchange.org) via the iProX partner repository (Ma et al., 2019) with the dataset identifier PXD033729. Microscopy data reported in this paper will be shared by the lead contact upon request
- This paper does not report original code.
- Any additional information required to reanalyze the data reported in this paper is available from the lead contact upon request.

Experimental model details

Mice—All mice were housed in a temperature- and humidity-controlled environments with free access to standard chow and water and on a 12 h/12 h light/dark cycle according to the guidelines of laboratory animal welfare and ethics committee of the Third Military Medical University. All mouse strains were maintained in the Third Military Medical University specific pathogen-free animal facility.

NG2-CreER.: These mice have been previously described (The Jackson Laboratory, 008538) (Zhu et al., 2011) and were crossed with R26-LSL-tdTomato mice (The Jackson Laboratory, 007908) (Madisen et al., 2010) to produce NG2-CreER:R26-LSL-tdTomato, or with tau-mGFP mice (The Jackson Laboratory, 021162)(Wang et al., 2020) to produce NG2-CreER:tau-mGFP mice. Mice were given 3 consecutive daily tamoxifen treatments via gavage at 10 mg/kg to induce Cre-mediated recombination and oligodendroglial lineage cell labeling.

Aldh1l1-eGFP.: These mice have been previously described (Molofsky et al., 2013). They were crossed with NG2-CreER:R26-LSL-tdTomato mice to produce Aldh1l1-eGFP:NG2-CreER:R26-LSL-tdTomato mice, which achieve astrocyte and OPC labelling after 2 consecutive daily tamoxifen treatments starting from P1 or P2.

DTA mice.: These mice have been described previously (The Jackson Laboratory, 009669) (Voehringer et al., 2008) and was crossed with hGFAP-Cre (The Jackson Laboratory, 024098) (Chung et al., 2013) mice or Cx3cr1-CreERT-YFP mice (The Jackson Laboratory, 021160) (Parkhurst et al., 2013) to generate hGFAP-Cre:DTA mice or Cx3cr1-CreERT-YFP:DTA mice and their non-cre:DTA/+ littermate control. hGFAP-Cre:DTA mice were subjected to experiment at P7. To induce DTA expression in Cx3cr1-CreERT-YFP:DTA mice, they were given 3 consecutive daily tamoxifen treatments from P4 to P6 and subjected to experiment at P10.

Aldh1l1-CreERT.: These mice previously described (The Jackson Laboratory, 031008) (Yu et al., 2018) were used for conditional gene knockdown experiments. Mice were subjected to AAV-injection in the cortex at P2, followed by 3 consecutive daily tamoxifen treatments, before subjected to experiments at P7.

Tetrodotoxin (TTX) injection model.: The experiment procedure was conducted as described previously (Demerens et al., 1996). The P4 mice were cold-anesthetized before the injection procedure. 0.5 μL 100 nM TTX (Sigma) was injected with a 10-μL Hamilton syringe, anterior to the corneoscleral junction into the vitreous humor of the right eye. The mice were monitored for half an hour before returned to their home cage, and were subjected to immunohistochemistry examination at P7.

SD Rats—All Rats were housed in a temperature- and humidity-controlled, pathogen-free environments with free access to standard chow and water and on a 12 h/12 h light/dark cycle, and subjected to experiments according to the guidelines of laboratory animal welfare and ethics committee of the Third Military Medical University.

Primary cell cultures

Primary rat OPC culture.: Primary rat OPCs were isolated as described previously (Niu et al., 2012). Briefly, the cerebral hemispheres of P0~3 rats were diced and dissociated with papain (Sigma), and the resulting cells were seeded in dulbecco's modified eagle medium (DMEM, Gibco) supplemented with 10% fetal bovine serum (FBS, Gibco) until cells were confluent. The medium was then switched to OPC proliferation medium for two days. Subsequently, the OPCs were detached using 0.5% EDTA, and cultured in OPC proliferation medium on PDL-coated surface or in other experiment conditions: onto monolayer EC, on PFA-fixed monolayer EC, or in 25% EC-conditioned medium. For differentiation assay, the OPC proliferation medium was switched to differentiation medium for 2 days before cell collection. For semaphorin treatment, 10~200 ng/mL semaphorins (mSema3a, mSema6a, or mSema7a, R&D, 5926-S3, 9017-S6, 1835-S3) were added to the OPC proliferation or differentiation medium. Cells were treated for 2 days before collected for immunostaining.

Primary rat endothelial cell culture.: Primary rat endothelial cells were isolated from P14 Sprague–Dawley rats as previously described (Sauer et al., 2005), and cultured on collagen type I and fibronectin-coated coverslips.

293T cell culture.: 293T cells (ATCC, CRL3216) were maintained in DMEM supplemented with 10% fetal bovine serum. For 293T cell and OPC co-culture, 293T cells were seeded onto PDL-coated coverslips in 24 well plate at 7500 cells/well, and culture for 24 h, followed by OPC seeding in differentiation medium. Cells were then maintained for 2 days before collected for immunostaining.

Method details

Immunohistochemistry—Mice were perfused intracardially with 4% PFA and the brain were cryoprotected in 30% sucrose and processed for 20 μm cryosections. Sections were permeated in 0.5% Triton-X100 in phosphate buffered saline (PBS), blocked with 2% bovine serum albumin (BSA), and incubated overnight at 4°C with primary antibodies. Sections were then washed thrice before secondary antibody incubation for 1 h at room temperature, following by thrice washes and mounting with coverslips. Primary antibodies used are: Rabbit anti-NeuN (Abcam, ab177487), Rabbit anti-BLBP (Abcam, ab32423), Goat anti-GFAP (Abcam, ab53554), Rabbit anti-NG2 (Millipore, MAB5320), Rabbit anti-ITPR2 (Millipore, AB3000), Goat anti-PDGFRα (R&D, AF1062), Mouse anti-Olig2 (Millipore, MABN50), Rabbit anti-Olig2 (Millipore, AB9610), Mouse anti-CC1 (Millipore, OP80), Rat anti-MBP (Millipore, MAB386), Rabbit anti-Iba1 (Wako, 019–19741), Rabbit anti-Ki67 (Thermo, MA514520), Goat anti-GFP (Abcam, ab5450), Rat anti-CD31 (BD Biosciences, 553370), Rat anti-PDGFRβ (Invitrogen, 14–1402-81), Rabbit anti-Sema3a (Abcam, ab23393), Rabbit anti-Sema6a (Abcam, ab154938), Rabbit anti-Sema7a (Abcam, ab23578), Rabbit anti-Plxna4 (Abcam, ab39350), Rat anti-Plxna2 (Thermo, MA524263), Goat anti-Plxnd1 (Abcam, ab28762). Dylight 488/594/649-conjugated Lectin (Vector Lab, DL-1174, DL-1177, DL-1178). Images were captured using VS200 Research Slide Scanner (Olympus), FV3000 confocal microscope (Olympus), Ixplore SpinSR confocal microscope (Olympus), or Axio Imager M2 with the apotome system (Zeiss). Super-resolution images were captured using Ixplore SpinSR confocal super resolution system with a UPLAPO60XOHR objective (Olympus).

Brain slices live imaging—The brain slices live imaging experiment was conducted as previously described with several modification (Sonego et al., 2013). Briefly, the P5 Aldh1l1-eGFP:NG2-CreER:R26-LSL-tdTomato mouse was sedated on ice and subjected to intravenous injection of 10 μL Dylight 649-conjugated Lectin (Vector Lab, DL-1178) before sacrifice. 300 μm brain slices were prepared by vibratome (Leica, VT1200) and transferred onto a 0.4 μm Millicell cell culture insert (Millipore, PICM0RG50), which was then lay onto the imaging medium in a 35 mm glass bottom dish (Nunc, 150680). The slices were allowed to equilibrate in the 37°C 95% O_2 5% CO_2 incubator for 1 h, and carried to the Ixplore SpinSR confocal microscope (Olympus) in a live imaging chamber maintained at 37°C with continuous 95% O_2 and 5% CO_2 input. 6 μm-interval Z-stacked live images were taken with a LUCPLFLN 20X/0.45 objective (Olympus) at a 15 min or 20 min interval.

***in vivo* live imaging—**The P5 Aldh1l1-eGFP:NG2-CreER:R26-LSL-tdTomato mouse was anesthetized and subjected to intravenous injection of 10 μL Dylight 649-conjugated Lectin (Vector Lab, DL-1178). The scalp of the mouse was removed, and a 1 mm diameter cranial window was opened above the area of interest. A drop of 0.9% saline was added to the cranial window before the attachment of a round coverslip. The mouse was then secured on the FV3000 confocal microscope and the live images were collected using a UPLSAPO30XS objective (Olympus) at a 20 min interval.

Two-photon laser ablation of astrocytes—The two-photon laser ablation experiment was conducted as previously described with several modification (Kubotera *et al.*, 2019). The P5 Aldh1l1-eGFP mouse was anesthetized and a cranial window was opened before the mouse was transferred to the Leica SP8 two-photon microscope. A 900 nm wavelength laser was used to visualize the eGFP-labeled astrocytes and to induce laser ablation. The high-power laser beam (45–115 mW) was scanned in a 5 μm × 5 μm area at the center of the target astrocyte for ~10 s to achieve ablation. The astrocyte ablation was conducted in a 200 μm (x) × 200 μm (y) × 100 μm (z) area ~50 μm below the pia surface. After the experiment, the revived pups were returned to their parent, and were sacrificed at P6 for immunohistochemistry experiment.

Immunopanning—Immunopanning experiment was carried out as previously described with some modifications (Foo, 2013). The rat or mouse brain was minced and digested with 1 mg/mL papain at 37°C for 1 h. After the cessation of digestion by ovomucoid (Worthington, LS003086), the resulting cell suspension was incubated with primary antibodies [astrocyte, mouse anti-ITGB5 (Invitrogen, 14–0497-82); OPC, rat anti-PDGFRα (BD Biosciences, 558774); OL, mouse anti-PLP (Millipore, MAB388); mouse microglia, rat anti-CD45 (BD, 550539); neuron, rabbit anti-p75 (Abcam, EP1039Y)] diluted in the panning buffer for 30 min at room temperature. The cell suspension was then transferred to a series of secondary antibodies coated 10-cm dishes, and incubated for 30 min. After attachment of the target cell types to the dish, the remnant cell suspension was removed, and the dish was washed with the panning buffer thrice. The cells were then collected with RIPA buffer and subjected to proteomic analysis.

Proteomic analysis—Immunopanning-obtained cells from 6 rats were pooled together for proteomic analysis, and 3 technical repeats were performed. Cells were lysed using RIPA, which was proteolyzed by trypsin and subjected to Tandem Mass Tag (TMT) labeling, before subjected to LC-MS / MS analysis. The resulting data were processed using the Maxquant (v1.5.2.8). Tandem mass spectra were searched against the UniProt Rat database. Trypsin/P was specified as the cleavage enzyme, allowing up to 2 missing cleavages. The mass error was set to 20 ppm and 5 ppm for precursor ions in First search and Main search, respectively, and 0.02 Da for fragment ions. Carbamidomethylation of cysteine residues was specified as a fixed modification, and methionine oxidation was specified as a variable modification. For the protein quantification method, TMT-6-plex was selected. The FDR was adjusted to < 1%.

The identified proteins were annotated by their subcellular localization using Wolfpsort (v.0.2). Astrocyte extracellular or plasma membrane proteins, as well as OPC/OL plasma

membrane proteins were subjected to subsequent analysis. To identify the astrocyte-enriched protein list, the identified astrocyte proteins were cross-referenced with astrocyte-enriched transcription profiling (Zhang et al., 2014). To obtained the OPC-enriched protein list, the identified OPC proteins were compared to the OL proteins, and the mean difference of 1.2-fold-change was considered cutoff of differential expressed proteins. Protein interaction analysis of astrocyte enriched extracellular/plasma membrane proteins and OPC enriched plasma membrane proteins, as well as their functional annotation, was performed using the STRING database (Szklarczyk et al., 2021). The data presentation was done using Cytoscape (Cline et al., 2007).

Adeno-associated virus (AAV) injection—To generate the Semaphorins conditional knockdown AAV, shRNAs targeting Sema3a, Sema6a, and Sema7a were inserted into the pAAV-CBG-DIO-mCherry(or eGFP)-miR30shRNA-WPRE vector and packaged into the AAV2/5 virus. 3 shRNA sequences were designed for each target gene as following: Sema3a, 5'-CCCAGTGTTTCCTATAAATAA-3', 5'-CCTGAAAGAATGTGCCAATTT-3', and 5'-GCCTTGGTATATTGGCAATTT-3'; Sema6a, 5'-GTATTTCGCATGGCAACTATA-3', 5'-CCAATGAGTTTCCCGATGATA-3', and 5'-CCTGAGAACAATGGTCAGATA-3'; Sema7a, 5'-ACTCAGCTGTCTGCGTGTATT-3', 5'-CCATAGCTTTGTCTTCAATAT-3', and 5'-GCAGGAATACAACGGGAAGAT-3'. Scramble shRNA sequence: 5'-GAAGTCGTGAGAAGTAGAA-3'. To generate the Sema3a conditional overexpression AAV, the mouse Sema3a coding sequence (2319 bp, NM_009152.4), along with a P2A sequence, was cloned into the pAAV-CMV-DIO-EGFP-tWPA vector, to generate the pAAV-CMV-DIO-Sema3a-P2A-EGFP-tWPA vector, which was then packaged into the AAV2/5 virus. The virus construction and packaging technical service was from OBiO, Shanghai. The virus was injected into the cortex of the P2 Aldh1l1-CreERT mice at the following coordinate: 1 mm rostral to the lambda point, 0.5 mm from the midline, insertion depth at 0.8 mm. 1 μL virus (with the titer of $4\sim8 \times 10^{12}$) was injected at the speed of 0.07 μL/min. To induce Cre-mediated recombination, the mice were treated with tamoxifen at 10 mg/kg body weight via gavage from P3 to P5.

Electron microscopy—The electron microscopy analysis was performed as previously described (Mei et al., 2013). Animals were initially anesthetized with 1% pentobarbital and transcardially perfused with 0.01 M phosphate buffer (PB). The cortex of hGFAP-Cre:DTA and control mice were rapidly removed and fixed with fresh 3% glutaraldehyde overnight at 48°C. Tissues were rinsed with PB, postfixed with 1% OsO4 in PB for 2 h, counterstained with uranyl acetate, dehydrated with a graded acetone series, infiltrated with propylene oxide, and embedded in Epon. Semithin sections (2 μm) or ultrathin sections (60 nm) were generated with an ultramicrotome (LKB-V, LKB Produkter AB, Bromma) and viewed under a light microscope (BX60, Olympus) or transmission electron microscope (TECNAI10, Philips), respectively. Three sections at comparable locations were investigated at a magnification of 80 kV.

Immunogold labelling—Mice were perfused intracardially with PBS followed by pre-cold 4% PFA and the brain were processed by Vibratome (submerged in 0.1 M PBS) to obtained 50 μm free-floating sections. Sections were postfixed with 4% PFA with 0.1%

glutaraldehyde in 0.1 M PB for 2 h, washed with 0.1 M PB for 10 min thrice. The residual fixatives were then quenched with 50 mM glycine in 0.1 M PB for 30 min. Sections were washed with 0.1 M PB for 10 min, permeabilized in 0.05% Triton-X100:PB for 15 min, washed again with 0.1 M pb for 15 min, and incubate in blocking buffer (0.1 M PBS with 0.1% BSA-CTM) for 1.5 h. Sections were then incubated with primary antibody (Goat anti-PDGFRα (1:300, R&D, AF1062)) at 4°C overnight, washed with blocking buffer 6 × 10 min, and incubated with 1.4-nm gold-conjugated secondary antibody (Nanoprobes) overnight. Sections were then washed with blocking buffer 6 × 10 min, 0.1 M PB 3 × 10 min, and postfixed in 2.5% glutaraldehyde for 4 h, followed by washing with 0.1 M PB 3 × 10 min, ddH_2O 6 × 5 min, Sodium Citrate (pH7.0) 3 × 5 min, before subjected to silver enhancement with the HQ Silver Kit (Nanoprobes). Immunolabelled sections were rinsed in ddH2O 6 × 10 min, post-fixed with 1% osmium tetroxide in PB for 1 h and then incubated in 2% uranyl acetate in ddH2O for 40 min in the dark. Sections were dehydrated in graded ethanol, then acetone series, and finally flat-embedded in Epon 812. After polymerization, flat-embedded sections were examined under a light microscope. Serial ultrathin (~70–90 nm) sections were cut with an Ultramicrotome (Leica EM UC6, Germany) using a diamond knife (Diatome) and mounted on formvar-coated mesh grids (6–8 sections per grid). They were observed under a Tecnai G2 Spirit 120 kV transmission electron microscopy at the Center of Cyro-Electron Microscopy, Zhejiang University.

***In situ* hybridization—**The *in situ* hybridization experiment was performed as previously described (Niu *et al.*, 2019). Briefly, anesthetized mice were perfused intracardially with 4% PFA and brain were collected cryoprotected in 30% sucrose with 0.1% diethyl pyrocarbonate, followed by cryosection. For *in situ* hybridization, sections were incubated with desdigoxigenin (DIG)-labeled antisense PLP probe at 65°C overnight, followed by 5 washes and then incubated with anti-Digoxigenin-AP Fab fragments antibody (1:1500, Sigma-Aldrich, 11093274910) at 4°C overnight. The targeted mRNA-expressing cells were visualized as a dark purple deposition with NBT/BCIP (nitro blue tetrazolium/5-bromo-4-chloro-3-indolyl phosphate)-alkaline phosphatase combination the following day.

Transwell migration assay—Primary rat OPC was seeded in the 24 well-format 8.0 μm Transwell insert (Corning, 353097), and cultured in 0.5 mL OPC proliferation medium. Semaphorins (mSema3a, mSema6a, and mSema7a) were added to the well outside the Transwell insert at 200 ng/mL. Cells were treated for 48 h before fixation with 75% Ethanol for 30 min at −20°C, and subjected to immunostaining.

RT-qPCR—Total RNA was isolated from immunopanning-isolated cells using Trizol according to the manufacturer’s protocol. The reverse transcription experiments were carried out using the PrimeScript RT Reagent Kit from Takara. The qPCR experiments were performed with the FastStart Universal SYBR Mix (Roche, 04913914001) and Accurate 96 Real Time PCR System (DLAB).

Quantification and statistical analysis

Quantifications

OPC quantification.: For the OPC–vessel association analysis, PDGFRα/CD31(or Lectin) double staining was used to detect the association of OPCs with blood vessels. The percentage of PDGFRα+ cells with their cell bodies directly in contact with blood vessels was quantified.

Quantification of astrocytic endfeet coverage.: To quantify Aldh1l1-GFP astrocytic endfeet coverage in embryonic stages, the length of vessel with endfeet and the length of total vessel were measured, and the ratio between them was analyzed. To quantify postnatal Aldh1l1-GFP astrocytic endfeet coverage, the Lectin-masked Aldh1l1-GFP+ area and the Lectin+ area was measured, and the ratio between them was calculated.

Fluorescent intensity and area quantifications.: To quantify fluorescent-positive area or intensity, the regions of interest were separated by setting a threshold at least two times the background. Cell counting and fluorescence intensity analyses were conducted on six randomly chosen fields for each sample using ImageJ.

Visualization of Semaphorin/Plexin staining within astrocyte/OPC domain.: This visualization procedure was conducted using Imaris as previously described (Schafer et al., 2014). The deconvoluted z-stacked images captured by a UPLAPO60XOHR objective (Olympus) were imported to Imaris software, where the Aldh1l1-eGFP+ astrocyte or PDGFRα+ OPC cell surfaces were constructed by threshold set to include the positive signals. The Semaphorin or Plexin signals were then masked by the astrocyte or OPC cell surfaces to exclude signals not within the cell volume. Figures S2F and S2G, lower panels present the maximum projected overlay of the Aldh1l1-GFP and masked Semophorins, or of the PDGFRα and masked Plexins, respectively. Likewise, Figures S3D, S3F, and S3H present the maximum projected overlay of viral-expressed eGFP/tdTomato and masked Semaphorin signal.

Colocalization test between Semaphorin/Plexin staining and Aldh1l1-eGFP/PDGFRα staining.: Similar as previously mentioned (Lehrman et al., 2018), the z-stacked images captured by a UPLAPO60XOHR objective (Olympus) were used. The pixel intensity correlation between Semaphorins and Aldh1l1-eGFP staining, as well as that between Plexins and PDGFRα staining, was calculated using Fiji colocalization analysis tool to obtain the Pearson's correlation coefficient. After initial measurement, the Semaphorin or Plexin channels were rotated 90°, followed by a second colocalization analysis, which serves as a negative control. Significant reduction of the Pearson's correlation coefficient after the channel rotation suggests high confidence of colocalization.

Quantification of Semaphorin staining in transfected astrocytes.: The z-stacked images captured by a UPLAPO60XOHR objective (Olympus) were used. The Semaphorin signal was masked by the positive signal of eGFP or tdTomato using the 3D counter analyzer in ImageJ (Fiji). The resulting masked image was projected with maximum signal. The ratio

between Semaphorin-positive area and total cell area was measured. At least 50 cells in each experimental repeat were quantified.

Statistical analysis—Statistical significance between groups was determined with GraphPad Prism software. The unpaired t-test was used to determine the significance between two experimental groups. One-way analysis of variance (ANOVA) was used to determine the significances among three and four groups. Pearson correlation test was used to determine the correlation between astrocyte endfoot formation and juxtavascular OPC percentage. Data distribution was assumed to be normal, but this was not formally tested. A probability of $P < 0.05$ was considered statistically significant. All significant statistical results are indicated within the figures with the following conventions: *$P < 0.05$, **$P < 0.01$, ***$P < 0.001$, ****$P < 0.0001$. Error bars represent ±standard deviation. No statistical methods were used to predetermine sample sizes. The sample size per group was determined from previous publications with similar methodology. Control mice and their littermate mutant mice were collected from different litters, and randomly selected for each experiment. Investigators were blinded to group allocation during data analysis. All experiments were performed at least three times, and the findings were replicated in individual mice and cell cultures in each experiment.

Supplementary Material

Refer to Web version on PubMed Central for supplementary material.

Acknowledgements

We thank reviewers for their important and thoughtful comments which helped us to improve our manuscript. This work was supported by grants from the National Key Research and Development Program of China (2021ZD0201703 to J.N. and L.X.), National Nature Science Foundation of China (NSFC 32070964 to J.N.; 81971309 and 32170980 to C.Y.), Guangdong Basic and Applied Basic Research Foundation (2022B1515020012 to C.Y.). Shenzhen Fundamental Research Program (JCYJ20190809161405495, JCYJ20210324123212035 and RCYX20200714114644167 to C.Y.). S.P.J.F. was supported by grants from NIH/NINDS (R01NS097551, P01NS083513, R21NS119954). S.P.J.F. is a Harry Weaver Neuroscience Scholar of the National Multiple Sclerosis Society.

References

Bernard F, Moreau-Fauvarque C, Heitz-Marchaland C, Zagar Y, Dumas L, Fouquet S, Lee X, Shao Z, Mi S, and Chedotal A (2012). Role of transmembrane semaphorin Sema6A in oligodendrocyte differentiation and myelination. Glia 60, 1590–1604. 10.1002/glia.22378. [PubMed: 22777942]

Binamé F, Pham-Van LD, Spenlé C, Jolivel V, Birmpili D, Meyer LA, Jacob L, Meyer L, Mensah-Nyagan AG, Po C, et al. (2019). Disruption of Sema3A/Plexin-A1 inhibitory signalling in oligodendrocytes as a therapeutic strategy to promote remyelination. EMBO molecular medicine 11, e10378. 10.15252/emmm.201910378. [PubMed: 31566924]

Boyd A, Zhang H, and Williams A (2013). Insufficient OPC migration into demyelinated lesions is a cause of poor remyelination in MS and mouse models. Acta neuropathologica 125, 841–859. 10.1007/s00401-013-1112-y. [PubMed: 23595275]

Cai J, Qi Y, Hu X, Tan M, Liu Z, Zhang J, Li Q, Sander M, and Qiu M (2005). Generation of oligodendrocyte precursor cells from mouse dorsal spinal cord independent of on Nkx6 regulation and Shh signaling. Neuron 45, 41–53. [PubMed: 15629701]

Chiou B, Neely E, Kallianpur A, and Connor JR (2019). Semaphorin4A causes loss of mature oligodendrocytes and demyelination in vivo. Journal of neuroinflammation 16, 28. 10.1186/s12974-019-1420-9. [PubMed: 30736794]

Cho AN, Jin Y, Kim S, Kumar S, Shin H, Kang HC, and Cho SW (2019). Aligned Brain Extracellular Matrix Promotes Differentiation and Myelination of Human-Induced Pluripotent Stem Cell-Derived Oligodendrocytes. ACS Appl Mater Interfaces 11, 15344–15353. 10.1021/acsami.9b03242. [PubMed: 30974942]

Chung WS, Clarke LE, Wang GX, Stafford BK, Sher A, Chakraborty C, Joung J, Foo LC, Thompson A, Chen C, et al. (2013). Astrocytes mediate synapse elimination through MEGF10 and MERTK pathways. Nature 504, 394–400. 10.1038/nature12776. [PubMed: 24270812]

Cline MS, Smoot M, Cerami E, Kuchinsky A, Landys N, Workman C, Christmas R, Avila-Campilo I, Creech M, Gross B, et al. (2007). Integration of biological networks and gene expression data using Cytoscape. Nature protocols 2, 2366–2382. 10.1038/nprot.2007.324. [PubMed: 17947979]

de Waard DM, and Bugiani M (2020). Astrocyte-Oligodendrocyte-Microglia Crosstalk in Astrocytopathies. Frontiers in cellular neuroscience 14, 608073. 10.3389/fncel.2020.608073. [PubMed: 33328899]

Demerens C, Stankoff B, Logak M, Anglade P, Allinquant B, Couraud F, Zalc B, and Lubetzki C (1996). Induction of myelination in the central nervous system by electrical activity. Proceedings of the National Academy of Sciences of the United States of America 93, 9887–9892. 10.1073/pnas.93.18.9887. [PubMed: 8790426]

Fallier-Becker P, Vollmer JP, Bauer HC, Noell S, Wolburg H, and Mack AF (2014). Onset of aquaporin-4 expression in the developing mouse brain. International journal of developmental neuroscience : the official journal of the International Society for Developmental Neuroscience 36, 81–89. 10.1016/j.ijdevneu.2014.06.001. [PubMed: 24915007]

Foo LC (2013). Purification of rat and mouse astrocytes by immunopanning. Cold Spring Harbor protocols 2013, 421–432. 10.1101/pdb.prot074211. [PubMed: 23637363]

Funfschilling U, Supplie LM, Mahad D, Boretius S, Saab AS, Edgar J, Brinkmann BG, Kassmann CM, Tzvetanova ID, Mobius W, et al. (2012). Glycolytic oligodendrocytes maintain myelin and long-term axonal integrity. Nature 485, 517–521. 10.1038/nature11007. [PubMed: 22622581]

Giraudon P, Vincent P, Vuaillat C, Verlaeten O, Cartier L, Marie-Cardine A, Mutin M, Bensussan A, Belin MF, and Boumsell L (2004). Semaphorin CD100 from activated T lymphocytes induces process extension collapse in oligodendrocytes and death of immature neural cells. Journal of immunology 172, 1246–1255. 10.4049/jimmunol.172.2.1246.

Glial cell development : basic principles and clinical relevance. (2001). In Jessen KR, and Richardson WD, eds. 2nd ed. ed. Oxford University Press.

Gutiérrez-Franco A, Costa C, Eixarch H, Castillo M, Medina-Rodríguez EM, Bribián A, de Castro F, Montalban X, and Espejo C (2016). Differential expression of sema3A and sema7A in a murine model of multiple sclerosis: Implications for a therapeutic design. Clinical immunology (Orlando, Fla.) 163, 22–33. 10.1016/j.clim.2015.12.005. [PubMed: 26686462]

Hughes EG, Kang SH, Fukaya M, and Bergles DE (2013). Oligodendrocyte progenitors balance growth with self-repulsion to achieve homeostasis in the adult brain. Nature neuroscience 16, 668–676. 10.1038/nn.3390. [PubMed: 23624515]

Jarjour AA, and Kennedy TE (2004). Oligodendrocyte precursors on the move: mechanisms directing migration. The Neuroscientist : a review journal bringing neurobiology, neurology and psychiatry 10, 99–105. 10.1177/1073858403260751. [PubMed: 15070484]

Jiang P, Chen C, Liu XB, Pleasure DE, Liu Y, and Deng W (2016). Human iPSC-Derived Immature Astroglia Promote Oligodendrogenesis by Increasing TIMP-1 Secretion. Cell Rep 15, 1303–1315. 10.1016/j.celrep.2016.04.011. [PubMed: 27134175]

Kessaris N, Fogarty M, Iannarelli P, Grist M, Wegner M, and Richardson WD (2006). Competing waves of oligodendrocytes in the forebrain and postnatal elimination of an embryonic lineage. Nature neuroscience 9, 173–179. 10.1038/nn1620. [PubMed: 16388308]

Kruger RP, Aurandt J, and Guan KL (2005). Semaphorins command cells to move. Nat Rev Mol Cell Biol 6, 789–800. 10.1038/nrm1740. [PubMed: 16314868]

Kubotera H, Ikeshima-Kataoka H, Hatashita Y, Allegra Mascaro AL, Pavone FS, and Inoue T (2019). Astrocytic endfeet re-cover blood vessels after removal by laser ablation. Sci Rep 9, 1263. 10.1038/s41598-018-37419-4. [PubMed: 30718555]

Lee Y, Morrison BM, Li Y, Lengacher S, Farah MH, Hoffman PN, Liu Y, Tsingalia A, Jin L, Zhang PW, et al. (2012). Oligodendroglia metabolically support axons and contribute to neurodegeneration. Nature 487, 443–448. 10.1038/nature11314. [PubMed: 22801498]

Lehrman EK, Wilton DK, Litvina EY, Welsh CA, Chang ST, Frouin A, Walker AJ, Heller MD, Umemori H, Chen C, and Stevens B (2018). CD47 Protects Synapses from Excess Microglia-Mediated Pruning during Development. Neuron 100, 120–134 e126. 10.1016/j.neuron.2018.09.017. [PubMed: 30308165]

Leslie JR, Imai F, Fukuhara K, Takegahara N, Rizvi TA, Friedel RH, Wang F, Kumanogoh A, and Yoshida Y (2011). Ectopic myelinating oligodendrocytes in the dorsal spinal cord as a consequence of altered semaphorin 6D signaling inhibit synapse formation. Development (Cambridge, England) 138, 4085–4095. 10.1242/dev.066076. [PubMed: 21831918]

Lu QR, Sun T, Zhu Z, Ma N, Garcia M, Stiles CD, and Rowitch DH (2002). Common developmental requirement for Olig function indicates a motor neuron/oligodendrocyte connection. Cell 109, 75–86. 10.1016/s0092-8674(02)00678-5. [PubMed: 11955448]

Luo Y, Raible D, and Raper JA (1993). Collapsin: a protein in brain that induces the collapse and paralysis of neuronal growth cones. Cell 75, 217–227. 10.1016/0092-8674(93)80064-l. [PubMed: 8402908]

Ma J, Chen T, Wu S, Yang C, Bai M, Shu K, Li K, Zhang G, Jin Z, He F, et al. (2019). iProX: an integrated proteome resource. Nucleic acids research 47, D1211–D1217. 10.1093/nar/gky869. [PubMed: 30252093]

Madisen L, Zwingman TA, Sunkin SM, Oh SW, Zariwala HA, Gu H, Ng LL, Palmiter RD, Hawrylycz MJ, Jones AR, et al. (2010). A robust and high-throughput Cre reporting and characterization system for the whole mouse brain. Nature neuroscience 13, 133–140. 10.1038/nn.2467. [PubMed: 20023653]

Mann F, Chauvet S, and Rougon G (2007). Semaphorins in development and adult brain: Implication for neurological diseases. Prog Neurobiol 82, 57–79. 10.1016/j.pneurobio.2007.02.011. [PubMed: 17537564]

Mei F, Wang H, Liu S, Niu J, Wang L, He Y, Etxeberria A, Chan JR, and Xiao L (2013). Stage-specific deletion of Olig2 conveys opposing functions on differentiation and maturation of oligodendrocytes. J Neurosci 33, 8454–8462. 10.1523/JNEUROSCI.2453-12.2013. [PubMed: 23658182]

Meyer-Franke A, Shen S, and Barres BA (1999). Astrocytes induce oligodendrocyte processes to align with and adhere to axons. Molecular and cellular neurosciences 14, 385–397. 10.1006/mcne.1999.0788. [PubMed: 10588392]

Miller RH (2002). Regulation of oligodendrocyte development in the vertebrate CNS. Prog Neurobiol 67, 451–467. 10.1016/s0301-0082(02)00058-8. [PubMed: 12385864]

Molofsky AV, Glasgow SM, Chaboub LS, Tsai HH, Murnen AT, Kelley KW, Fancy SP, Yuen TJ, Madireddy L, Baranzini S, et al. (2013). Expression profiling of Aldh1l1-precursors in the developing spinal cord reveals glial lineage-specific genes and direct Sox9-Nfe2l1 interactions. Glia 61, 1518–1532. 10.1002/glia.22538. [PubMed: 23840004]

Moore CS, Abdullah SL, Brown A, Arulpragasam A, and Crocker SJ (2011). How factors secreted from astrocytes impact myelin repair. Journal of neuroscience research 89, 13–21. 10.1002/jnr.22482. [PubMed: 20857501]

Niu J, Tsai HH, Hoi KK, Huang N, Yu G, Kim K, Baranzini SE, Xiao L, Chan JR, and Fancy SPJ (2019). Aberrant oligodendroglial-vascular interactions disrupt the blood-brain barrier, triggering CNS inflammation. Nature neuroscience 22, 709–718. 10.1038/s41593-019-0369-4. [PubMed: 30988524]

Niu J, Wang L, Liu S, Li C, Kong J, Shen HY, and Xiao L (2012). An efficient and economical culture approach for the enrichment of purified oligodendrocyte progenitor cells. Journal of neuroscience methods 209, 241–249. 10.1016/j.jneumeth.2012.05.032. [PubMed: 22687939]

Nutma E, van Gent D, Amor S, and Peferoen LAN (2020). Astrocyte and Oligodendrocyte Cross-Talk in the Central Nervous System. Cells 9. 10.3390/cells9030600.

Okada A, Tominaga M, Horiuchi M, and Tomooka Y (2007). Plexin-A4 is expressed in oligodendrocyte precursor cells and acts as a mediator of semaphorin signals. Biochemical

and biophysical research communications 352, 158–163. 10.1016/j.bbrc.2006.10.176. [PubMed: 17109816]

Parkhurst CN, Yang G, Ninan I, Savas JN, Yates JR 3rd, Lafaille JJ, Hempstead BL, Littman DR, and Gan WB (2013). Microglia promote learning-dependent synapse formation through brain-derived neurotrophic factor. Cell 155, 1596–1609. 10.1016/j.cell.2013.11.030. [PubMed: 24360280]

Piaton G, Aigrot MS, Williams A, Moyon S, Tepavcevic V, Moutkine I, Gras J, Matho KS, Schmitt A, Soellner H, et al. (2011). Class 3 semaphorins influence oligodendrocyte precursor recruitment and remyelination in adult central nervous system. Brain 134, 1156–1167. 10.1093/brain/awr022. [PubMed: 21421691]

Sauer I, Dunay IR, Weisgraber K, Bienert M, and Dathe M (2005). An apolipoprotein E-derived peptide mediates uptake of sterically stabilized liposomes into brain capillary endothelial cells. Biochemistry 44, 2021–2029. 10.1021/bi048080x. [PubMed: 15697227]

Schafer DP, Lehrman EK, Heller CT, and Stevens B (2014). An engulfment assay: a protocol to assess interactions between CNS phagocytes and neurons. Journal of visualized experiments : JoVE. 10.3791/51482.

Schneider CA, Rasband WS, and Eliceiri KW (2012). NIH Image to ImageJ: 25 years of image analysis. Nat Methods 9, 671–675. 10.1038/nmeth.2089. [PubMed: 22930834]

Sonego M, Zhou Y, Oudin MJ, Doherty P, and Lalli G (2013). In vivo postnatal electroporation and time-lapse imaging of neuroblast migration in mouse acute brain slices. J Vis Exp. 10.3791/50905.

Spassky N, de Castro F, Le Bras B, Heydon K, Quéraud-LeSaux F, Bloch-Gallego E, Chédotal A, Zalc B, and Thomas JL (2002). Directional guidance of oligodendroglial migration by class 3 semaphorins and netrin-1. J Neurosci 22, 5992–6004. 10.1523/jneurosci.22-14-05992.2002. [PubMed: 12122061]

Sugimoto Y, Taniguchi M, Yagi T, Akagi Y, Nojyo Y, and Tamamaki N (2001). Guidance of glial precursor cell migration by secreted cues in the developing optic nerve. Development (Cambridge, England) 128, 3321–3330. [PubMed: 11546748]

Syed YA, Hand E, Möbius W, Zhao C, Hofer M, Nave KA, and Kotter MR (2011). Inhibition of CNS remyelination by the presence of semaphorin 3A. J Neurosci 31, 3719–3728. 10.1523/jneurosci.4930-10.2011. [PubMed: 21389227]

Szklarczyk D, Gable AL, Nastou KC, Lyon D, Kirsch R, Pyysalo S, Doncheva NT, Legeay M, Fang T, Bork P, et al. (2021). The STRING database in 2021: customizable protein-protein networks, and functional characterization of user-uploaded gene/measurement sets. Nucleic acids research 49, D605–d612. 10.1093/nar/gkaa1074. [PubMed: 33237311]

Takamatsu H, and Kumanogoh A (2012). Diverse roles for semaphorin-plexin signaling in the immune system. Trends in immunology 33, 127–135. 10.1016/j.it.2012.01.008. [PubMed: 22325954]

Tekki-Kessaris N, Woodruff R, Hall AC, Gaffield W, Kimura S, Stiles CD, Rowitch DH, and Richardson WD (2001). Hedgehog-dependent oligodendrocyte lineage specification in the telencephalon. Development (Cambridge, England) 128, 2545–2554. [PubMed: 11493571]

Tognatta R, Karl MT, Fyffe-Maricich SL, Popratiloff A, Garrison ED, Schenck JK, Abu-Rub M, and Miller RH (2020). Astrocytes Are Required for Oligodendrocyte Survival and Maintenance of Myelin Compaction and Integrity. Frontiers in cellular neuroscience 14, 74. 10.3389/fncel.2020.00074. [PubMed: 32300294]

Tsai HH, Frost E, To V, Robinson S, Ffrench-Constant C, Geertman R, Ransohoff RM, and Miller RH (2002). The chemokine receptor CXCR2 controls positioning of oligodendrocyte precursors in developing spinal cord by arresting their migration. Cell 110, 373–383. 10.1016/s0092-8674(02)00838-3. [PubMed: 12176324]

Tsai HH, Niu J, Munji R, Davalos D, Chang J, Zhang H, Tien AC, Kuo CJ, Chan JR, Daneman R, and Fancy SP (2016). Oligodendrocyte precursors migrate along vasculature in the developing nervous system. Science (New York, N.Y.) 351, 379–384. 10.1126/science.aad3839. [PubMed: 26798014]

Voehringer D, Liang HE, and Locksley RM (2008). Homeostasis and effector function of lymphopenia-induced “memory-like” T cells in constitutively T cell-depleted mice. Journal of immunology 180, 4742–4753. 10.4049/jimmunol.180.7.4742.

Wang F, Ren SY, Chen JF, Liu K, Li RX, Li ZF, Hu B, Niu JQ, Xiao L, Chan JR, and Mei F (2020). Myelin degeneration and diminished myelin renewal contribute to age-related deficits in memory. Nature neuroscience 23, 481–486. 10.1038/s41593-020-0588-8. [PubMed: 32042174]

Williams A, Piaton G, Aigrot MS, Belhadi A, Théaudin M, Petermann F, Thomas JL, Zalc B, and Lubetzki C (2007). Semaphorin 3A and 3F: key players in myelin repair in multiple sclerosis? Brain 130, 2554–2565. 10.1093/brain/awm202. [PubMed: 17855378]

Willis CM, Nicaise AM, Bongarzone ER, Givogri M, Reiter CR, Heintz O, Jellison ER, Sutter PA, TeHennepe G, Ananda G, et al. (2020). Astrocyte Support for Oligodendrocyte Differentiation can be Conveyed via Extracellular Vesicles but Diminishes with Age. Sci Rep 10, 828. 10.1038/s41598-020-57663-x. [PubMed: 31964978]

Xia W, and Fancy SPJ (2021). Mechanisms of oligodendrocyte progenitor developmental migration. Developmental neurobiology 81, 985–996. 10.1002/dneu.22856. [PubMed: 34643996]

Xiang X, Zhang X, and Huang QL (2012). Plexin A3 is involved in semaphorin 3F-mediated oligodendrocyte precursor cell migration. Neuroscience letters 530, 127–132. 10.1016/j.neulet.2012.09.058. [PubMed: 23063687]

Yamaguchi W, Tamai R, Kageura M, Furuyama T, and Inagaki S (2012). Sema4D as an inhibitory regulator in oligodendrocyte development. Molecular and cellular neurosciences 49, 290–299. 10.1016/j.mcn.2011.12.004. [PubMed: 22198439]

Yu X, Taylor AMW, Nagai J, Golshani P, Evans CJ, Coppola G, and Khakh BS (2018). Reducing Astrocyte Calcium Signaling In Vivo Alters Striatal Microcircuits and Causes Repetitive Behavior. Neuron 99, 1170–1187.e1179. 10.1016/j.neuron.2018.08.015. [PubMed: 30174118]

Zhang Y, Chen K, Sloan SA, Bennett ML, Scholze AR, O'Keeffe S, Phatnani HP, Guarnieri P, Caneda C, Ruderisch N, et al. (2014). An RNA-sequencing transcriptome and splicing database of glia, neurons, and vascular cells of the cerebral cortex. J Neurosci 34, 11929–11947. 10.1523/jneurosci.1860-14.2014. [PubMed: 25186741]

Zhu X, Hill RA, Dietrich D, Komitova M, Suzuki R, and Nishiyama A (2011). Age-dependent fate and lineage restriction of single NG2 cells. Development (Cambridge, England) 138, 745–753. 10.1242/dev.047951. [PubMed: 21266410]

Highlights

1. Astrocyte endfoot placement terminates developmental OPC perivascular migration.
2. Astrocyte-derived semaphorins 3a and 6a act to repel OPCs from blood vessels.
3. OPC detachment from endothelium permits their subsequent differentiation.

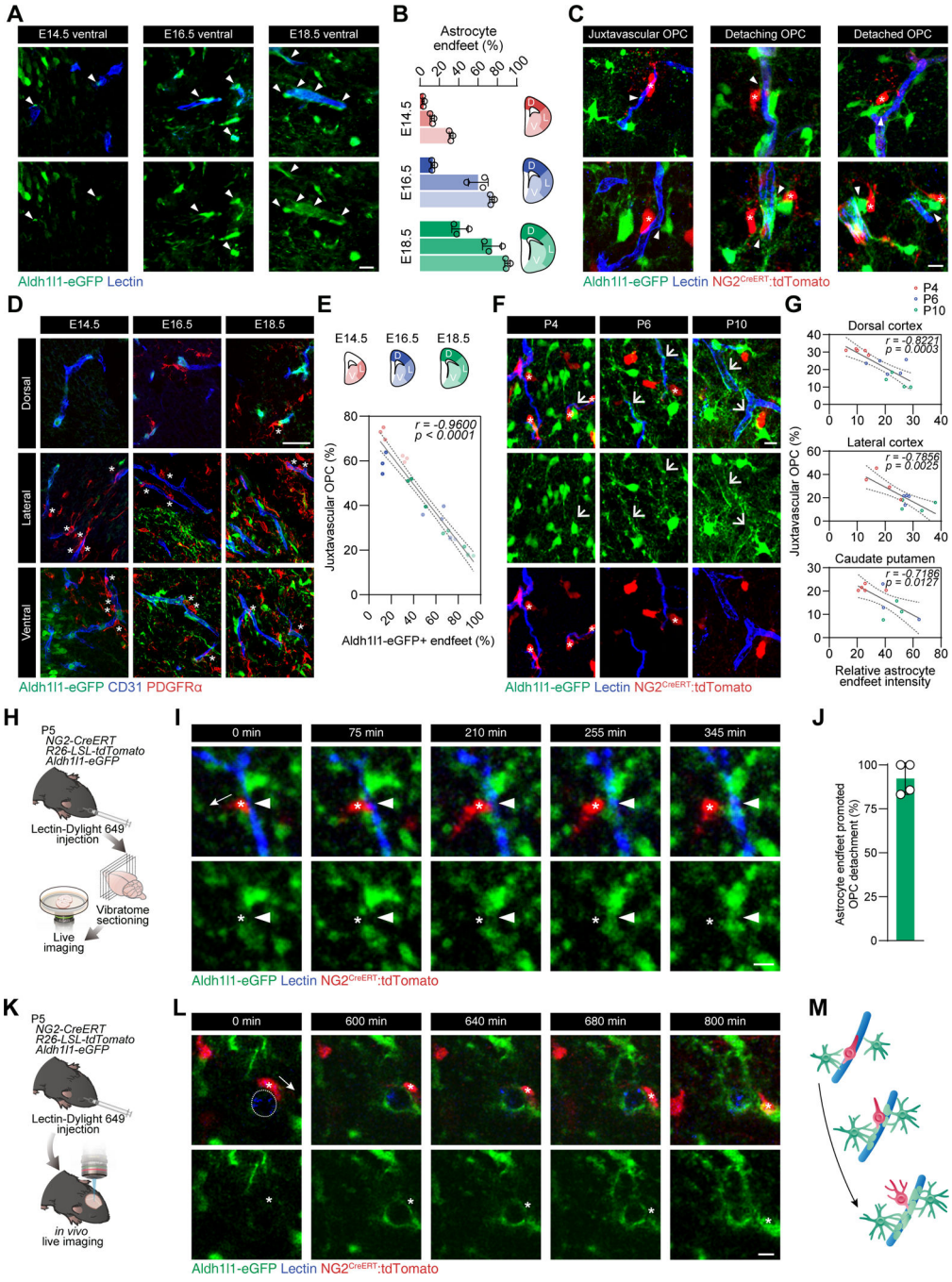

Figure 1. Astrocyte endfoot formation correlates with the termination of OPC perivascular migration and mediates OPC vascular detachment.

(A) Images of ventral forebrain of Aldh1l1-eGFP mice stained with Lectin at E14.5, E16.5, and E18.5. Arrowheads highlight astrocyte endfeet. Scale bar, 50 μm.

(B) Quantification of astrocyte endfeet covered percentage of vessel in dorsal, lateral, or ventral forebrain, at E14.5, E16.5, and E18.5.

(C) Images of brain section of P5 Aldh1l1-eGFP:NG2-CreER:R26-LSL-tdTomato mice intravenously injected with Lectin-AF649. tdTomato+ OPCs were attached to vessels devoid

of GFP+ astrocyte endfeet (left), and appeared to be displaced from the vessel by astrocyte endfeet (middle and right). Arrowheads highlight astrocyte endfeet. Scale bar, 10 μm

(D) Image of dorsal, lateral, and ventral forebrain of Aldh1l1-eGFP mice stained with Lectin and PDGFRα. Asterisks: juxtavascular OPC. Scale bar, 50 μm.

(E) Negative correlation between juxtavascular OPC percentage and astrocyte endfeet covered percentage was found among different brain regions and stages during embryonic development. Solid and dashed lines represent the simple linear regression and the 95% confidence intervals.

(F) Images of dorsal cortex of Aldh1l1-eGFP:NG2-CreER:R26-LSL-tdTomato mice at P4, P6 and P10. Arrows: astrocyte endfeet. Asterisks: juxtavascular OPC. Scale bar, 10 μm.

(G) juxtavascular OPC percentage was negatively correlated with astrocyte endfeet intensity on vessel among different stages in different brain regions during postnatal development. Solid and dashed lines represent the simple linear regression and the 95% confidence intervals.

(H) For acute brain slice live imaging, Lectin-AF649 was injected into the retro-orbital sinus of P5 Aldh1l1-eGFP:NG2-CreER:R26-LSL-tdTomato mice, followed by acute brain slice preparation and live imaging.

(I) Example of astrocyte endfeet displacing OPC (asterisk) from the vessel in live imaging. Arrows: migration direction. Arrowhead: the invading astrocyte endfeet. Asterisk: OPC. Scale bar: 10 μm.

(J) Quantification of OPC detaching events with astrocyte endfeet involvement. n = 4 experiments.

(K) For *in vivo* live imaging, following Lectin-AF649 injection, the mouse scalp was removed and an optical window was opened on the skull.

(L) Astrocyte endfeet-triggered OPC detachment observed *in vivo*. Arrows show the migration direction. Asterisk: OPC. Scale bar: 10 μm.

(M) Hypothesized positional relationships among OPCs, astrocytes and vessels during development. Red: OPC; Green: astrocyte; Blue: vessel.

n = 3 mice or 4 independent experiments.

See also Figure S1

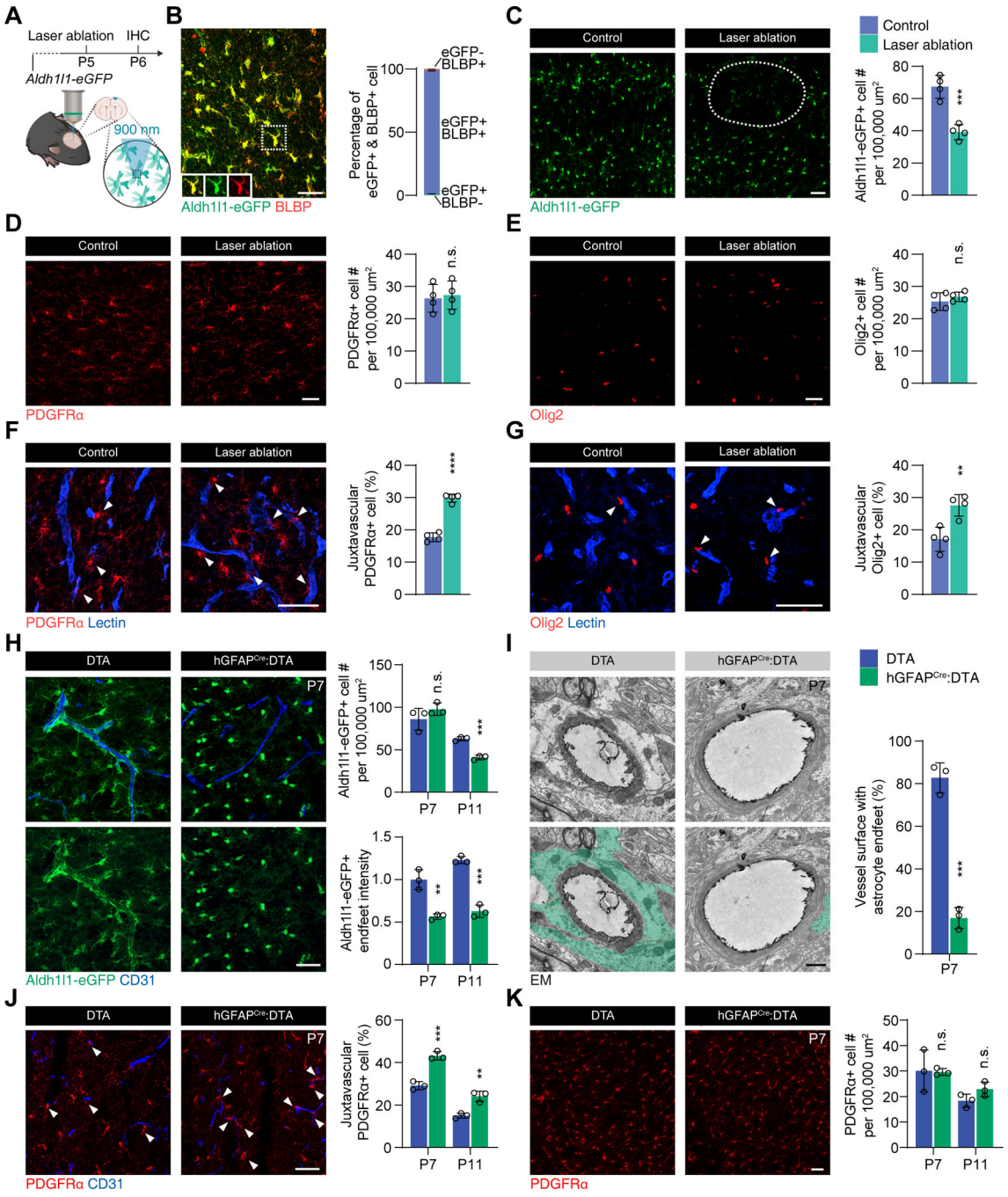

Figure 2. Experimental ablation of astrocytes suppresses OPC detachment from vasculature.

(A) P5 Aldh1l1-eGFP mice was subjected to laser ablation by two-photon microscopy to remove astrocytes in the dorsal cortical region.

(B) Staining of BLBP in Aldh1l1-eGFP mouse brain slice and quantification of the astrocyte-labeling efficiency of Aldh1l1-eGFP.

(C) Compared to the contralateral side, the laser ablation procedure successfully achieved focal astrocyte removal. Dash line delineates the laser ablated area.

(D) Laser ablation does not affect the number of PDGFRα+ OPCs.

(E) Laser ablation does not affect the number of Olig2+ oligodendroglia.
(F) Laser ablation of astrocytes led to an increased percentage of juxtavascular PDGFRα+ OPCs.
(G) Laser ablation of astrocytes led to an increased percentage of juxtavascular Olig2+ oligodendroglia.
(H) hGFAP-Cre:DTA:Aldh1l1-GFP mice showed reduced astrocyte number at P11 but not P7. However, the astrocyte endfoot formation was hindered as early as P7.
(I) Electron microscopy experiment at P7 confirms that hGFAP-Cre:DTA:Aldh1l1-GFP mice have lower astrocyte endfeet coverage on the vessels. Scale bar, 1 μm. Green color is added to highlight astrocyte endfeet.
(J, K) hGFAP-Cre:DTA mice showed increased juxtavascular OPC percentage at both P7 and P11, but did not cause a significant difference in the number of total OPCs. Scale bar, 50 μm except panel **(I)**. Bar plots represent mean ± standard deviation. n = 3 or 4 animals. * $p<0.05$, ** $p<0.01$, *** $p<0.001$, **** $p<0.0001$, n.s., not significant.
See also Figure S1

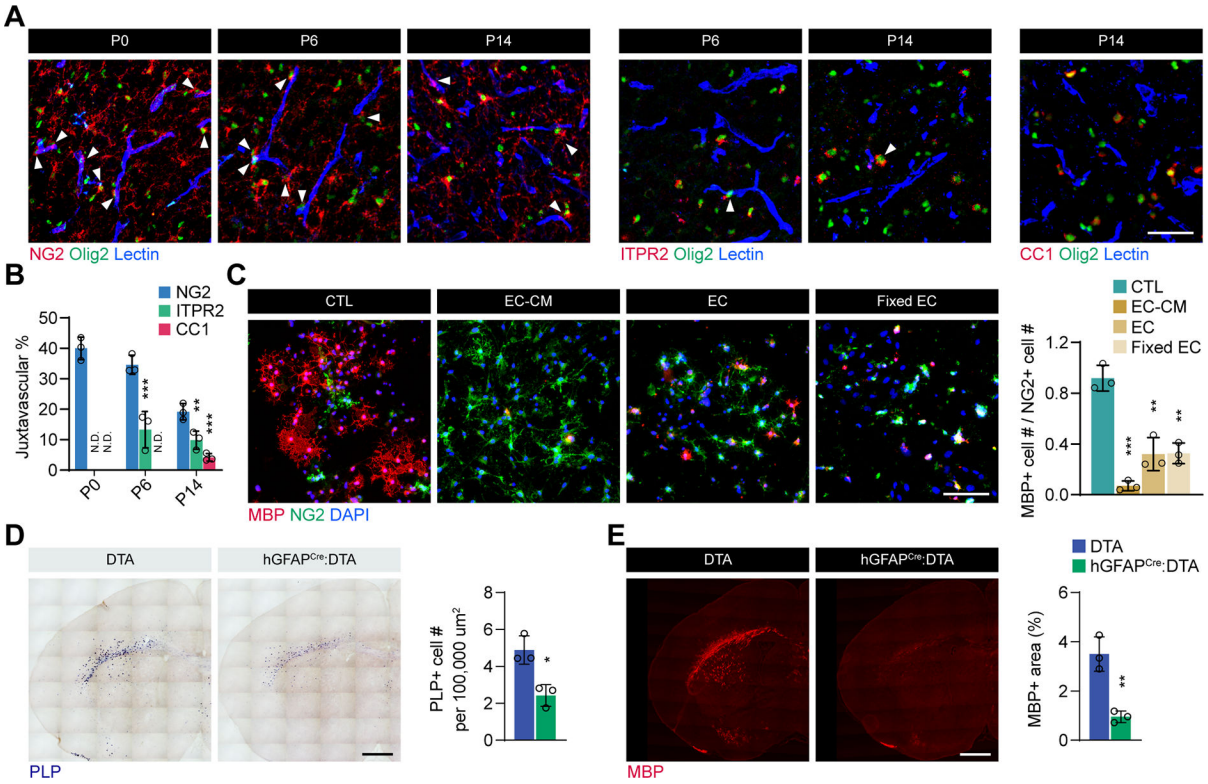

Figure 3. OPC detachment from vasculature permits their subsequent differentiation.

(A) Images of NG2, ITPR2, CC1 staining with Olig2 and Lectin counter stain in P0, P6, P14 dorsal cortex. Arrowheads indicate cells attached to the vessels as determined by the contact or overlap of their cell body to the vessel. Scale bar, 50 μm.

(B) Quantification of Juxtavascular NG2+, ITPR2+ or CC1+ cells in the dorsal cortex of P0, P6 and P14 mice. n = 3 animals. N.D., none (positive cell) detected.

(C) Primary OPCs were cultured in differentiation medium with endothelial cell conditioned medium (EC-CM), with endothelial cell (EC) co-cultures, or on fixed EC, followed by MBP and NG2 immunostaining. Ratio between MBP+ and NG2+ cell number was quantified. CTL, control. n = 3 experiments. Scale bar, 50 μm.

(D) *in situ* hybridization showed that DM20/PLP mRNA expression was reduced in hGFAP-Cre:DTA mice. Scale bar, 500 μm.

(E) Immunostaining showing that MBP expression was reduced in hGFAP-Cre:DTA mice. Scale bar, 500 μm. n = 3 animals. Bar plots represent mean ± standard deviation. * $p<0.05$, ** $p<0.01$, *** $p<0.001$.

See also Figure S1

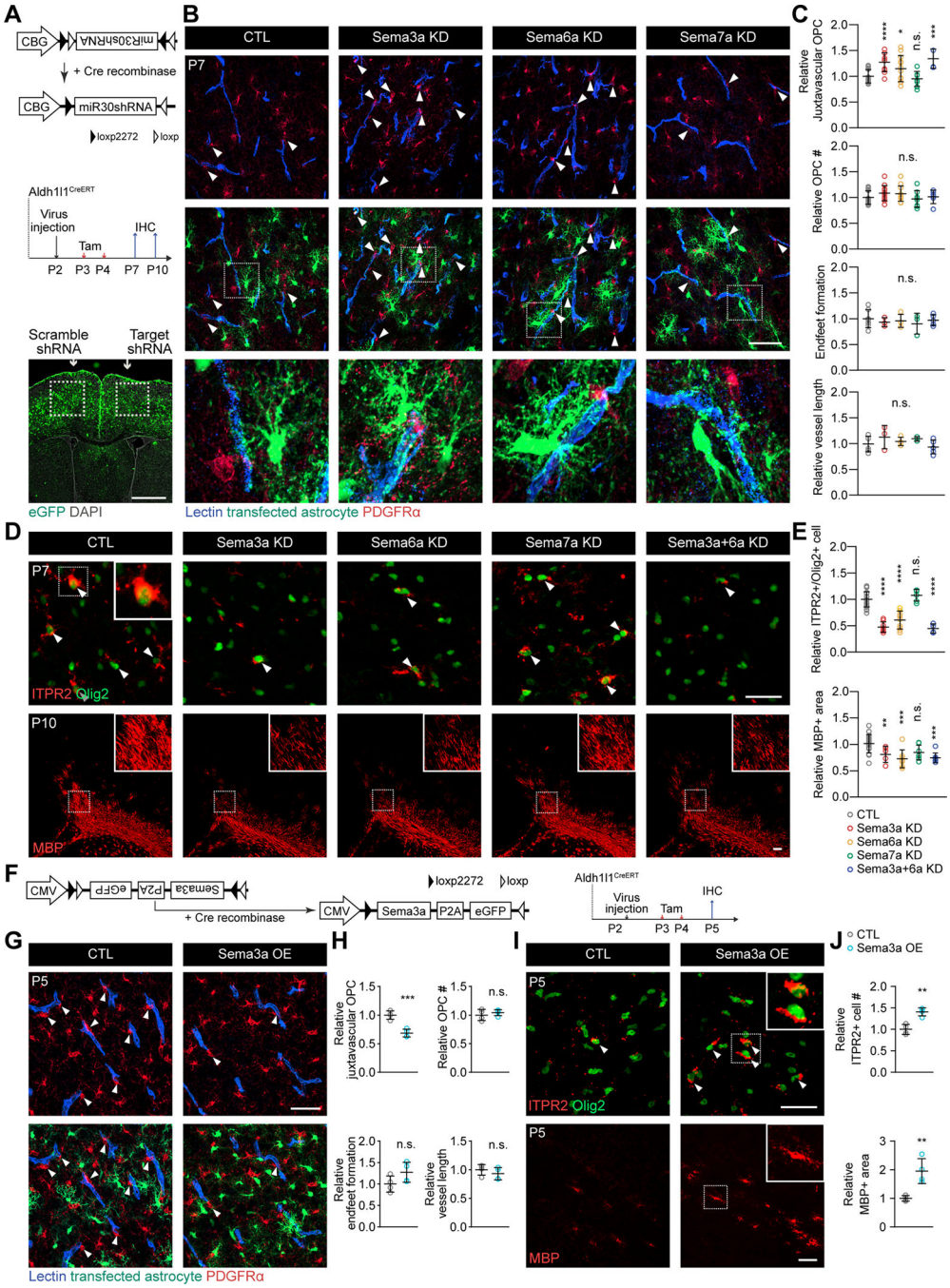

Figure 4. Astrocytes induce detachment of OPCs from vessels through semaphorin-plexin interactions.

(A) Semaphorin shRNAs were cloned into the miR30shRNA AAV vector with DIO elements. AAV was injected into the Aldh1l1-CreERT mice cortex at P2, followed by Tamoxifen induction at P3 and P4, and histological analysis at P7 or P10. Lower panel: GFP signals indicate successful virus injection and cre-recombination. Dash line square delineate the area of interest.

(B) Representative image of eGFP- or mCherry-labeled transfected astrocytes (with green pseudocolor) with Lectin and PDGFRα staining. Arrowheads highlight the juxtavascular OPCs. Scale bar, 50 μm. Lower panel, higher magnification image of the white squared region.
(C) Statistical analysis of juxtavascular OPC percentage, OPC number, vessel length and endfeet formation of transfected astrocytes in each group.
(D) Upper panel: representative images of ITPR2 and Olig2 staining in the P7 dorsal cortex of control and Semaphorin KD virus injected groups. Lower panel: representative images of MBP staining in the P10 cortex. Scale bar, 50 μm.
(E) Upper panel: quantification of the percentage of ITPR2-labeled Olig2+ cells, the newly formed OLs. Lower panel: quantification of MBP+ area percentage in the dorsal cortex.
(F) In the conditional overexpression AAV, the Sema3a-P2A-eGFP open-reading frame is controlled by a CMV promoter and flanked by DIO elements, allowing Aldh1l1-CreERT-induced astrocyte-specific Sema3a overexpression (Sema3a OE). AAV were injected into the Aldh1l1-CreERT mice cortex at P2, followed by Tamoxifen induction at P3 and P4, and histological analysis at P5.
(G) Representative image of eGFP-labeled transfected astrocytes with Lectin and PDGFRα staining. Arrowheads highlight the juxtavascular OPCs. Scale bar, 50 μm.
(H) Statistical analysis of juxtavascular OPC percentage, OPC number, vessel length and endfeet formation of transfected astrocytes in control and Sema3a OE cortex.
(I) Upper panel: representative images of ITPR2 and Olig2 staining in the P5 dorsal cortex of control and Sema3a OE virus injected groups. Lower panel: representative images of MBP staining in the P5 white matter. Scale bar, 50 μm.
(J) Upper panel: quantification of the percentage of ITPR2-labeled Olig2+ cells, the newly formed OLs. Lower panel: quantification of MBP+ area percentage in the white matter.
Dot plot represent mean ± standard deviation. Data are presented as fold change to control. n.s. not significant, n≥4 experiments. * $p<0.05$, ** $p<0.01$, *** $p<0.001$, **** $p<0.0001$.
See also Figures S2 and S3

Key resources table

REAGENT or RESOURCE	SOURCE	IDENTIFIER
Antibodies		
Rabbit anti-NeuN	Abcam	Cat# ab177487
Rabbit anti-BLBP	Abcam	Cat# ab32423
Goat anti-GFP	Abcam	Cat# ab5450
Rabbit anti-Sema3a	Abcam	Cat# ab23393
Rabbit anti-Sema6a	Abcam	Cat# ab154938
Rabbit anti-Sema7a	Abcam	Cat# ab23578
Rabbit anti-Plxna4	Abcam	Cat# ab39350
Goat anti-Plxnd1	Abcam	Cat# ab28762
Rabbit anti-p75	Abcam	Cat# EP1039Y
Goat anti-IBA1	Abcam	Cat# ab5076
Mouse anti-Human Nucleus Antigen	Abcam	Cat# ab191181
Rat anti-CD31	BD Biosciences	Cat# 553370
Rat anti-PDGFRα	BD Biosciences	Cat# 558774
Rat anti-CD45	BD Biosciences	Cat# 550539
Rabbit anti-NG2	Millipore	Cat# MAB5320
Rabbit anti-ITPR2	Millipore	Cat# AB3000
Mouse anti-Olig2	Millipore	Cat# MABN50
Rabbit anti-Olig2	Millipore	Cat# AB9610
Mouse anti-CC1	Millipore	Cat# OP80
Rat anti-MBP	Millipore	Cat# MAB386
Mouse anti-PLP	Millipore	Cat# MAB388
Rabbit anti-SOX10	Millipore	Cat# AB5727
Goat anti-PDGFRα	R&D	Cat# AF1062
Mouse anti-ITPR2	Santa Cruz	Cat# sc-398434
Sheep anti-Digoxigenin-AP Fab fragments	Sigma-Aldrich	Cat# 11093274910
Rabbit anti-Ki67	Thermo	Cat# MA514520
Rat anti-PDGFRβ	Thermo	Cat# 14–1402-81
Rat anti-Plxna2	Thermo	Cat# MA524263
mouse anti-ITGB5	Thermo	Cat# 14–0497-82
Dylight 488-conjugated Lectin	Vector Lab	Cat# DL-1174
Dylight 594-conjugated Lectin	Vector Lab	Cat# DL-1177
Dylight 649-conjugated Lectin	Vector Lab	Cat# DL-1178
Rabbit anti-IBA1	Wako	Cat# 019–19741
Bacterial and virus strains		
pAAV-CBG-DIO-mCherry-miR30shRNA(Sema3a-1)-WPRE	This paper; OBiO	N/A
pAAV-CBG-DIO-mCherry-miR30shRNA(Sema3a-2)-WPRE	This paper; OBiO	N/A
pAAV-CBG-DIO-mCherry-miR30shRNA(Sema3a-3)-WPRE	This paper; OBiO	N/A

REAGENT or RESOURCE	SOURCE	IDENTIFIER
pAAV-CBG-DIO-eGFP-miR30shRNA(Sema6a-1)-WPRE	This paper; OBiO	N/A
pAAV-CBG-DIO-eGFP-miR30shRNA(Sema6a-2)-WPRE	This paper; OBiO	N/A
pAAV-CBG-DIO-eGFP-miR30shRNA(Sema6a-3)-WPRE	This paper; OBiO	N/A
pAAV-CBG-DIO-mCherry-miR30shRNA(Sema7a-1)-WPRE	This paper; OBiO	N/A
pAAV-CBG-DIO-mCherry-miR30shRNA(Sema7a-2)-WPRE	This paper; OBiO	N/A
pAAV-CBG-DIO-mCherry-miR30shRNA(Sema7a-3)-WPRE	This paper; OBiO	N/A
pAAV-CBG-DIO-mCherry-miR30shRNA(scramble)-WPRE	OBiO	N/A
pAAV-CBG-DIO-eGFP-miR30shRNA(scramble)-WPRE	OBiO	N/A
pAAV-CMV-DIO-EGFP-tWPA	OBiO	N/A
pAAV-CMV-DIO-Sema3a-P2A-EGFP-tWPA	This paper; OBiO	N/A
Chemicals, peptides, and recombinant proteins		
Mouse Sema3a	R&D	Cat# 5926-S3
Mouse Sema6a	R&D	Cat# 9017-S6
Mouse Sema7a	R&D	Cat# 1835-S3
Tamoxifen	Sigma Aldrich	Cat# T5648
Critical commercial assays		
PrimeScript RT Reagent Kit	Takara	Cat# RR037A
FastStart Universal SYBR Mix	Roche	Cat# 04913914001
NBT/BCIP Stock Solution	Sigma-Aldrich	Cat# 11681451001
Deposited data		
Proteomics data	This paper; iProX	PXD033729
Experimental models: Cell lines		
293T	ATCC	Cat# CRL3216
Experimental models: Organisms/strains		
Mouse: NG2-CreER	The Jackson Laboratory	JAX: 008538
Mouse: R26-LSL-tdTomato	The Jackson Laboratory	JAX: 007908
Mouse: tau-mGFP	The Jackson Laboratory	JAX: 021162
Mouse: Aldh1l1-eGFP	The Jackson Laboratory	JAX: 030247
Mouse: DTA	The Jackson Laboratory	JAX: 009669
Mouse: hGFAP-Cre	The Jackson Laboratory	JAX: 024098
Mouse: Cx3cr1-CreERT-YFP	The Jackson Laboratory	JAX: 021160
Mouse: Aldh1l1-CreERT	The Jackson Laboratory	JAX: 031008
Mouse: C56BL/6j wild type	Animal breeding center of TMMU	N/A
Oligonucleotides		
Mouse Nrp1 F: CCACAGAGAAGCCAACCATTA	This paper	N/A
Mouse Nrp1 R: TGGCAGAATGTCTTGTGAGAG	This paper	N/A
Mouse Plxna1 F: TGTACTGAAGGAGATGGAGGT	This paper	N/A
Mouse Plxna1 R: CTAGTGTGCGGATGAAGGTTAG	This paper	N/A
Mouse Plxna2 F: GAACTGGAGGTACAGGGAAATG	This paper	N/A

REAGENT or RESOURCE	SOURCE	IDENTIFIER
Mouse Plxna2 R: CGGATGAAGGTCAGCAAGAA	This paper	N/A
Mouse Plxna4 F: GGAGTTTGTTCAGAGGGTATGT	This paper	N/A
Mouse Plxna4 R: CAGTGGTGTCAGGAATAGGAAG	This paper	N/A
Mouse Plxnc1 F: ACTGGATGTCTGTCTGTCTCT	This paper	N/A
Mouse Plxnc1 R: CCACGGGACCCTTGTTTATT	This paper	N/A
Mouse Plxnd1 F: CCTGACTAAAGCCACCTTCTT	This paper	N/A
Mouse Plxnd1 R: CAGCGGACCAGTGAGTTATT	This paper	N/A
Mouse Sema3a F: AGATTCATCAGTGCCCATCTC	This paper	N/A
Mouse Sema3a R: CCAGAGTGTTCTCCGTCTATTG	This paper	N/A
Mouse Sema4d F: CTCCTTGCTTCCATCTCTCATC	This paper	N/A
Mouse Sema4d R: CCCAACTACCCAACCCATTT	This paper	N/A
Mouse Sema6a F: TTAAACCCTGCCCTCCATTC	This paper	N/A
Mouse Sema6a R: ACCCAGCCTTCAGCATTAC	This paper	N/A
Mouse Sema6d F: CGTCAAGGAATACCAGCAGAA	This paper	N/A
Mouse Sema6d R: ACGGCCATGGACTTTGTATC	This paper	N/A
Mouse Sema7a F: TGGAGAGATACCAGGGTCTATG	This paper	N/A
Mouse Sema7a R: GGTACGGAAGACTCTGTCAATG	This paper	N/A
Mouse Gapdh F: AGGTCGGTGTGAACGGATTTG	This paper	N/A
Mouse Gapdh R: TGTAGACCATGTAGTTGAGGTCA	This paper	N/A
Software and algorithms		
Fiji/ImageJ	(Schneider et al., 2012)	https://imagej.nih.gov/ij/
cellSens	Olympus	N/A
Bitplane Imaris	Oxford Instruments	N/A
Maxquant (v1.5.2.8)	Max Planck Institute of Biochemistry	https://www.maxquant.org/
Wolfpsort (v.0.2)	N/A	https://wolfpsort.hgc.jp/
STRING database	(Szklarczyk *et al.*, 2021)	N/A
Cytoscape	(Cline et al., 2007)	N/A